Electronic Supplementary Material (ESI) for Environmental Science: Nano.
This journal is © The Royal Society of Chemistry 2019

Coupled Morphological and Structural Evolution of δ-MnO_2 to α-MnO_2 through Multistage Oriented Assembly Processes: the Role of Mn(III)

Xinran Liang,[a, b] Jeffrey E. Post,[c] Bruno Lanson,[d] Xiaoming Wang,[a] Mengqiang Zhu,[e] Fan Liu,[a] Wenfeng Tan,[a] Xionghan Feng,[a*] Guomin Zhu,[b] Xin Zhang,[b] James. J. De Yoreo[b]

a Key Laboratory of Arable Land Conservation (Middle and Lower Reaches of Yangtse River), Ministry of Agriculture, College of Resources and Environment, Huazhong Agricultural University, Wuhan 430070, China

b Physical Sciences Division, Pacific Northwest National Laboratory, Richland, WA 99352 United States

c Department of Mineral Sciences, Smithsonian Institution, Washington, DC 20013, USA

d University of Grenoble Alpes, CNRS, ISTerre, F-38000 Grenoble, France

e Department of Ecosystem Science and Management, University of Wyoming, Laramie, WY, 82071, United States.

Supporting Figures

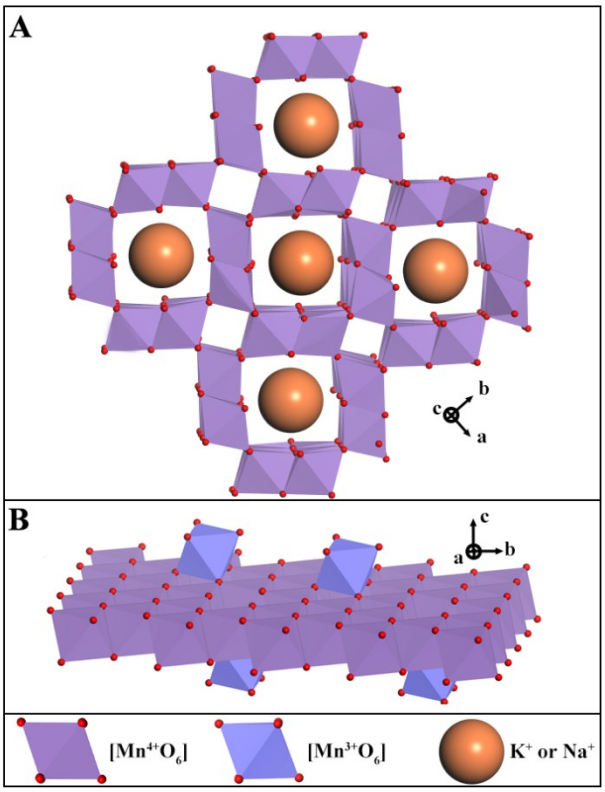

Figure S1. (A) α-MnO_2 [MnO_6] octahedra tunnel structure model; (B) δ-MnO_2 [MnO_6] octahedra layer structure model.

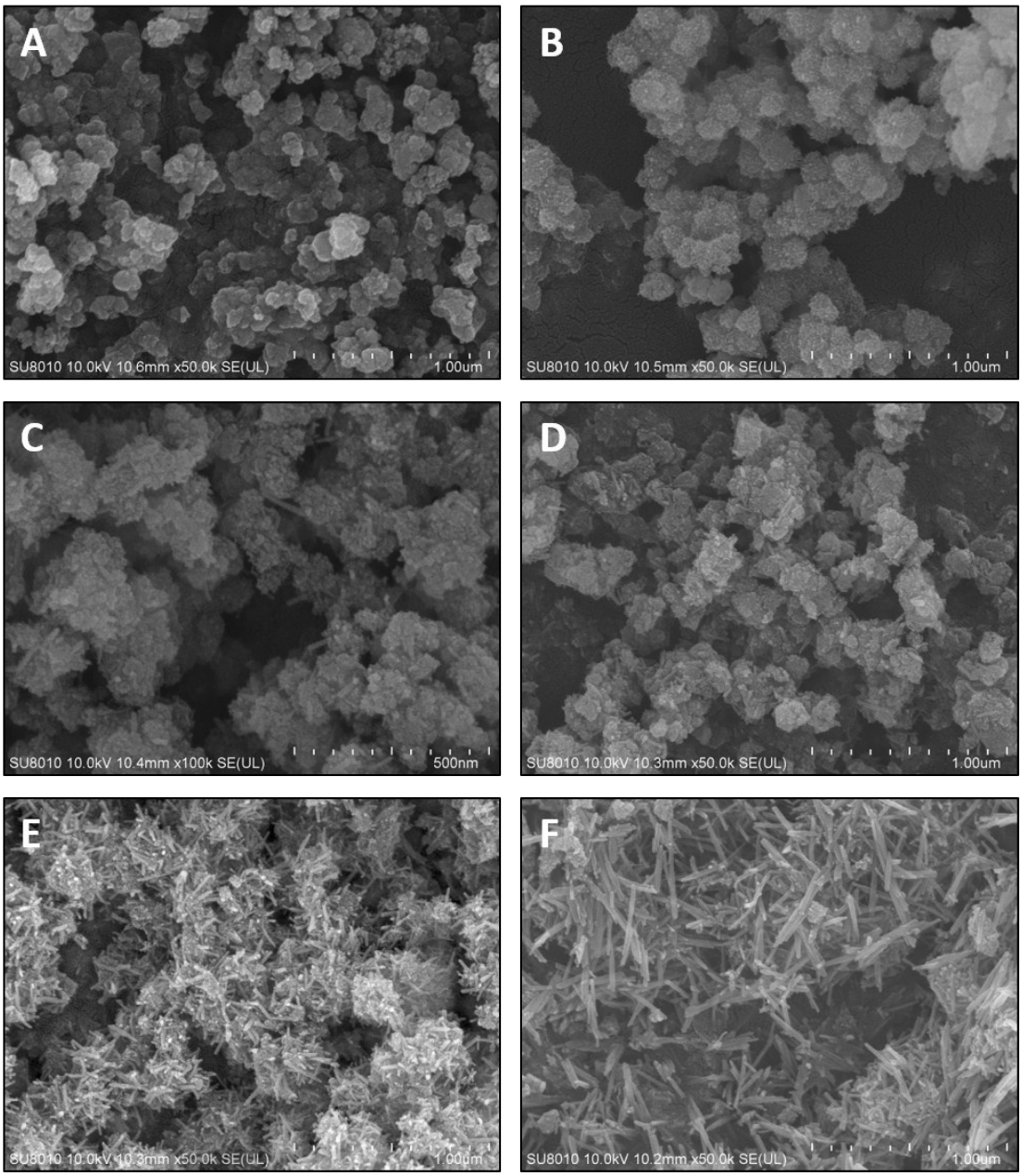

Figure S2. FESEM of intermediate product of (A) NaMix, (B) Na100-2, (C) Na100-6, (D) Na100-10, (E) Na 100-14 and (F) Na80.

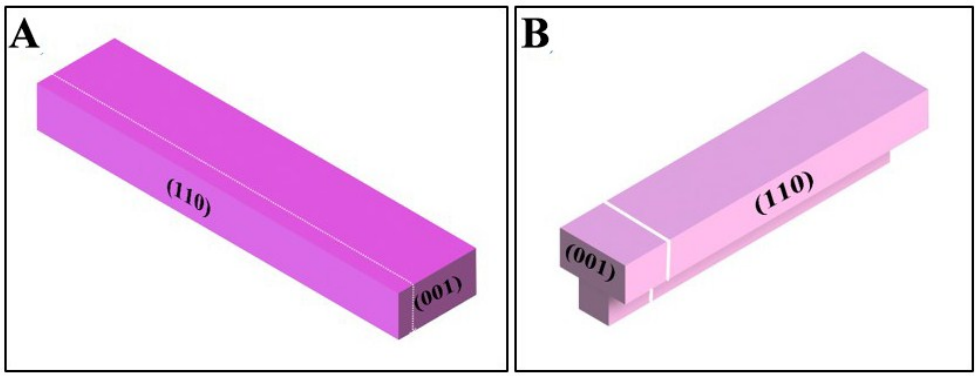

Figure S3. (A) The long nanosheets are cut along (001) plane, (B) The nanorods are cut along (001) plane.

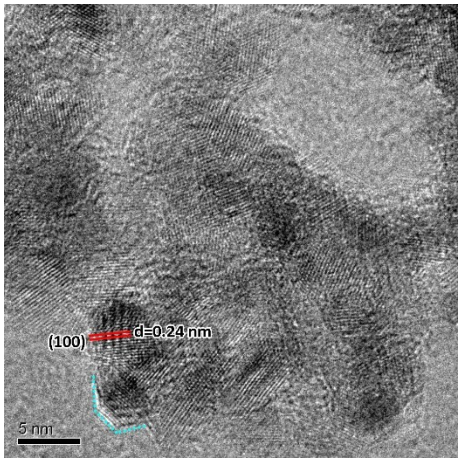

Figure S4. HRTEM image of the initial NaMix indicate the size about the edge of primary nanoflakes to be 3-4 nm

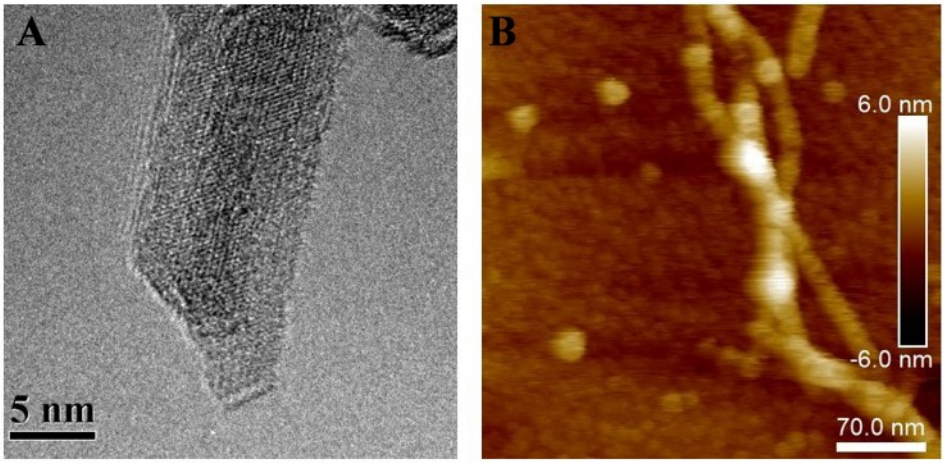

\

Figure S5. (A) HRTEM image of the intermediate Na100-10 indicate two long nanosheets stack and thicken. (B) AFM image of the intermediate Na100-10 indicate the nanoflakes stack on the nanoribbon.

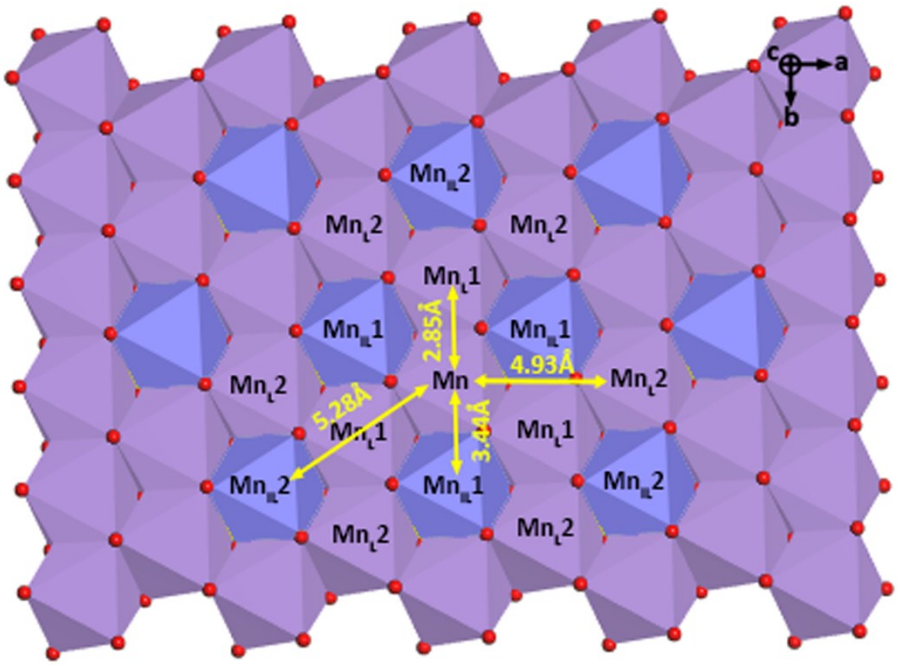

Figure S6. Scheme of a δ-MnO_2 layer which containing 1/3 vacancy (blue octahedral) per layer octahedron, seen along c-axis. The Mn_LX (X = 1, 2 or 3) means the first, second and third Mn shells around a given Mn. The $Mn_{IL}Y$ (Y= 1 or 2) means pairs formed by layer Mn and Mn at vacancies belonging respectively to the first and second shells.

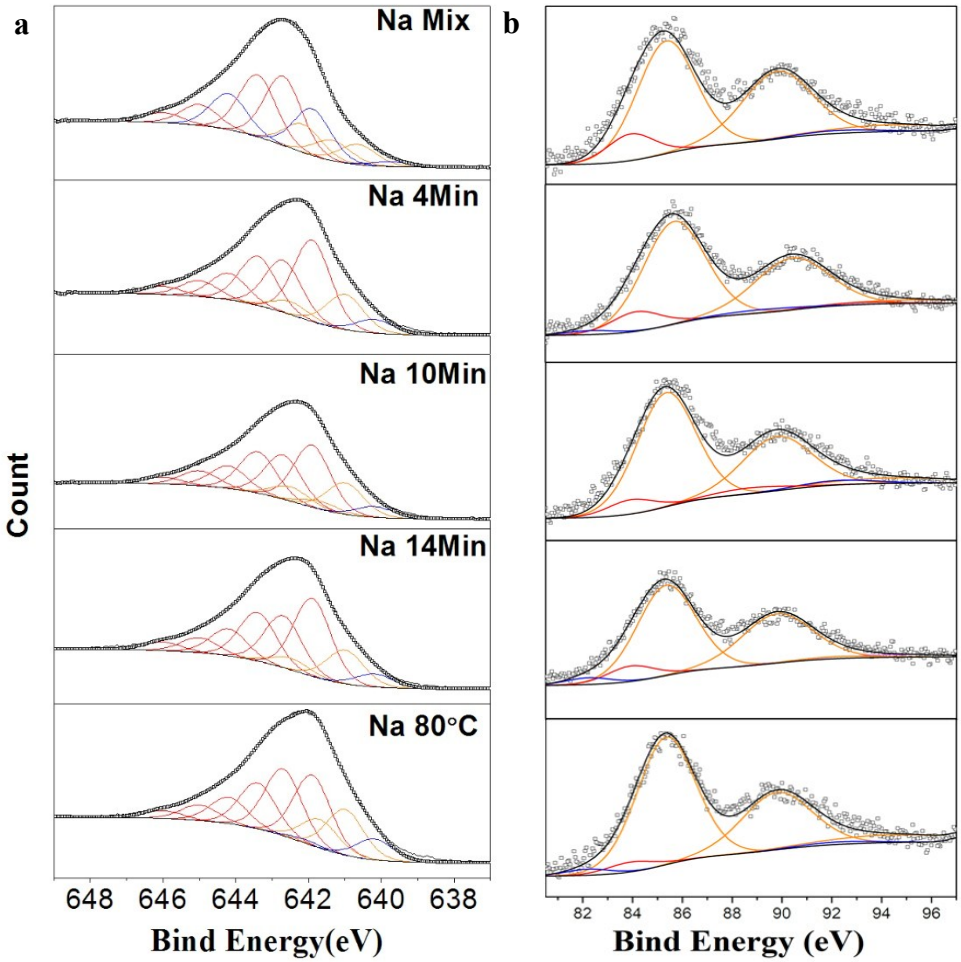

Figure S7. XPS broad scans of (a) Mn $2p_{3/2}$ and (b) Mn 3s spectra of intermediate products at NaMix, Na100-4, Na100-10, Na100-14, and Na80.

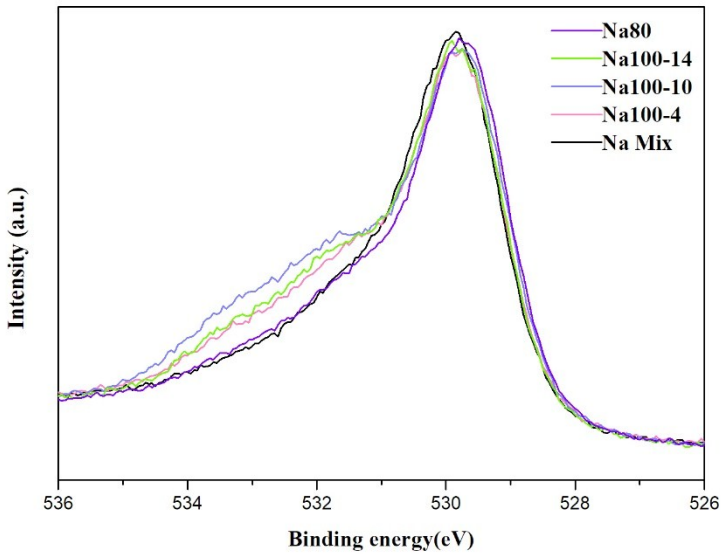

Figure S8. Oxygen 1s spectra of intermediate products at different intervals of Na+ stabilized α-MnO_2 formation and crystal growth;

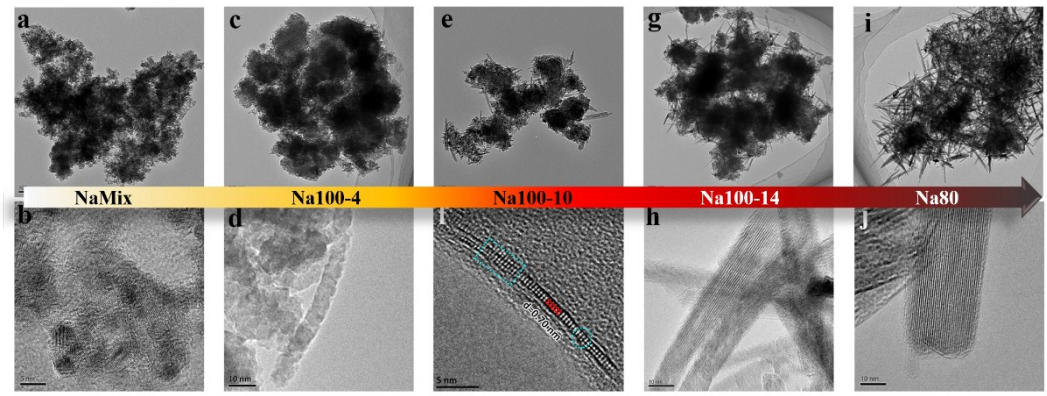

Figure S9. The TEM and HRTEM images during entire synthetic process: (a, b) NaMix, (c, d) Na100-4, (e, f) Na100-10, (g, h) Na100-14 and (i, j) Na80.

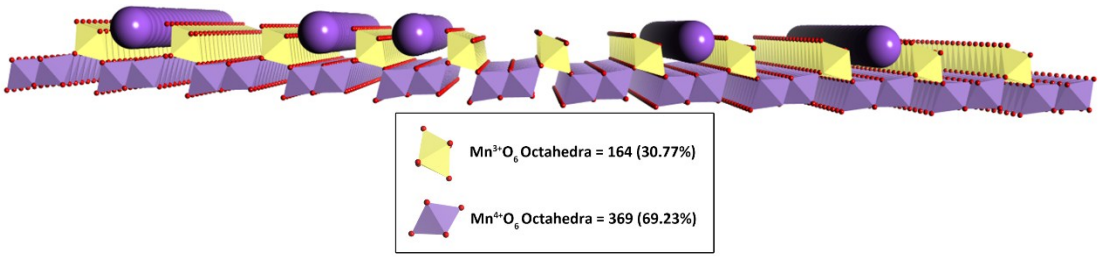

Figure S10. Schematic illustrating the ideal structure of δ-MnO_2 which can assemble to α-MnO_2.

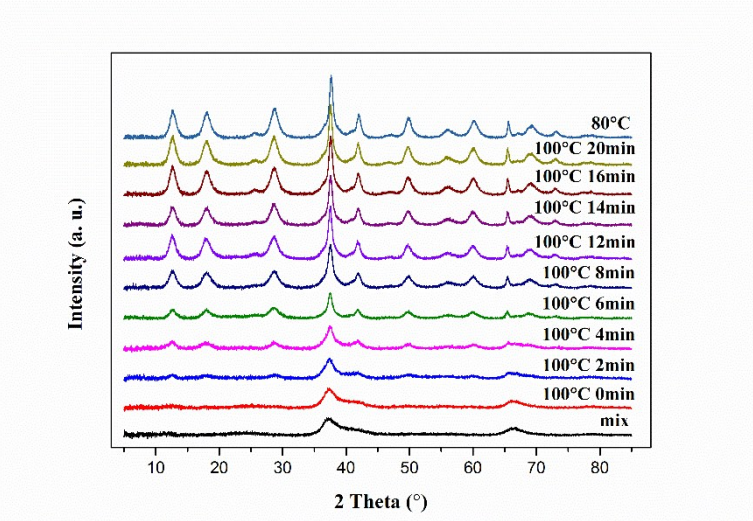

Figure S11. XRD patterns of intermediate products at different intervals of K^+ stabilized α-MnO_2 formation and crystal growth;

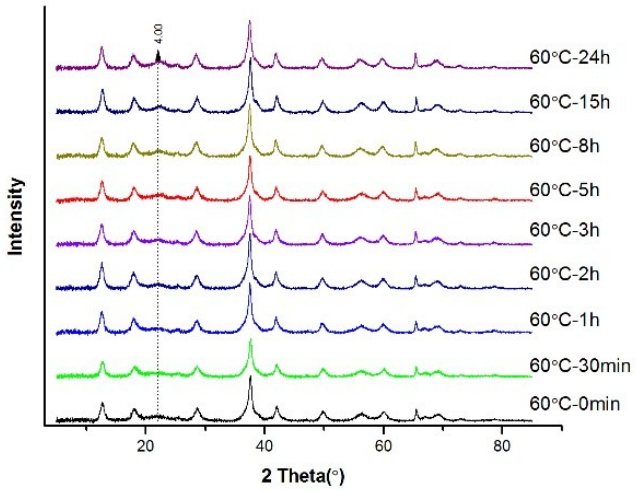

Figure S12. XRD patterns of intermediate products at different intervals of Na^+ stabilized α-MnO_2 age under 60 ℃.

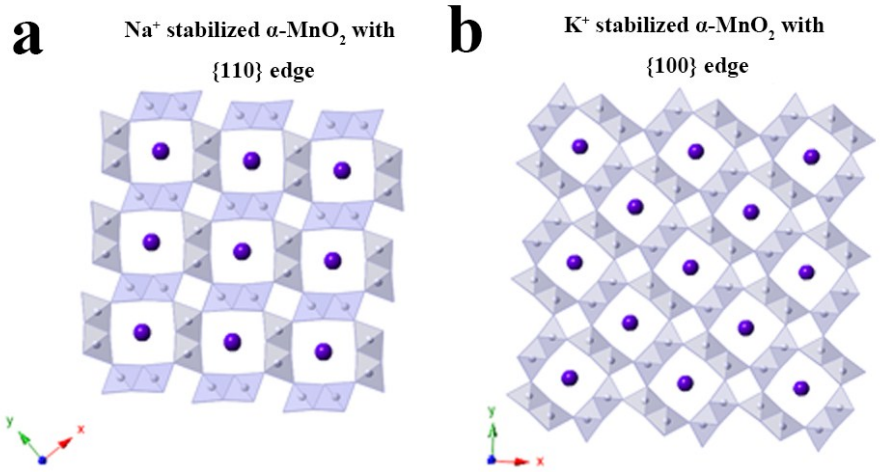

Figure S13 the calculated relaxed (a) Na^+ stabilized α-MnO_2 structure and (b) K^+ stabilized α-MnO_2 structure.

Supporting Tables

Table S1. K^+ content, average oxidation states (AOS) of Mn in intermediate products at various time intervals during K^+-stabilized α-MnO_2 formation obtained from titration and fittings of Mn ($2p^{3/2}$)

Samples	XPS (± 0.02)	Titration	K^+ content (% mol)
KMix	3.80	3.95 ± 0.03	6.91 ± 0.13
K100-0	3.77	3.90 ± 0.01	4.85 ± 0.09
K100-2	-	3.85 ± 0.01	39.57 ± 0.15
K100-4	3.74	3.80 ± 0.02	5.25 ± 0.11

K100-10	3.80	3.87 ± 0.04	5.89 ± 0.04
K100-20	-	3.85 ± 0.02	8.51 ± 0.03
K80	3.80	3.82 ± 0.03	10.56 ± 0.08

Table S2. Near-surface compositions of Mn and O species derived from fittings of Mn (2p3/2) and O (1s).

Sample	Mn(III) (±0.003)	Mn(II) (±0.001)	Mn(IV) (±0.003)	O^{2-}	OH^-	H_2O
KMix	0.158	0.037	0.845	0.661	0.183	0.156
K100-0	0.149	0.037	0.814	0.645	0.196	0.159
K100-4	0.153	0.049	0.798	0.580	0.218	0.202
K100-10	0.112	0.039	0.849	0.640	0.210	0.150
K80	0.137	0.028	0.835	0.770	0.161	0.068